Journal of Advanced Ceramics
2019, **8**(1): 121–132
https://doi.org/10.1007/s40145-018-0300-6
ISSN 2226-4108
CN 10-1154/TQ

Research Article

Enhanced mechanical properties and thermal shock resistance of Si_2BC_3N ceramics with SiC coated MWCNTs

Ning LIAO[a,b,*], Dechang JIA[a,b,*], Zhihua YANG[a,b], Yu ZHOU[a,b]

[a]*Institute for Advanced Ceramics*, *School of Materials Science and Engineering*, *Harbin Institute of Technology*, *Harbin 150080*, *China*
[b]*Key Laboratory of Advanced Structure-Function Integrated Materials and Green Manufacturing Technology*, *Ministry of Industry and Information Technology*, *Harbin 150080*, *China*

Received: July 1, 2018; Revised: October 9, 2018; Accepted: October 16, 2018

Abstract: Bulk Si_2BC_3N ceramics were reinforced with SiC coated multi-walled carbon nanotubes (MWCNTs). The phase compositions, mechanical properties, and thermal shock resistance, as well as the oxidation resistance of the designed Si_2BC_3N ceramics were comparatively investigated. The results show that nano SiC coating can be formed on MWCNTs through pyrolyzing polysilazane, which improves the oxidation resistance of MWCNTs. A stronger chemical bonding is formed between the SiC coated MWCNTs and SiC particles, contributing to improved flexural strength (532.1 MPa) and fracture toughness (6.66 MPa·$m^{1/2}$). Besides, the 2 vol% SiC coated MWCNTs reinforced Si_2BC_3N ceramics maintains much higher residual strength (193.0 MPa) after thermal shock test at 1000 ℃. The enhanced properties should be attributed to: (1) the breaking of MWCNTs and the debonding between MWCNTs and SiC interfaces, which leads to more energy dissipation; (2) the rough surfaces of SiC coated MWCNTs increase the adhesion strength during the "pull out" of MWCNTs.

Keywords: Si_2BC_3N ceramics; SiC coated MWCNTs; mechanical properties; thermal shock resistance

1 Introduction

As one of the high temperature structural ceramics, SiBCN ceramics have attracted intensive attentions due to their extraordinary high temperature stability up to 2000 ℃ without apparent decomposition [1–3]. With taking mechanical alloying (MA) together with sintering process, the dense bulk SiBCN ceramics can be prepared [4–6]. It was revealed that the fiber (C_f or SiC_f) reinforced SiBCN ceramics can be a potential candidate for applications at leading edges and nose-cones for a next generation of sharp re-entry space vehicles and for the thermal protection material [7,8]. However, there are still many obstacles in front of the practical applications. The main focuses were to improve the resistance to mechanical stress and thermochemical erosion. The former works have revealed the positive enhancing effects of additives, including ZrO_2 [9], AlN [10], Zr [11], Al [12], Zr + Al [13], LaB_6 [14,15], C_f [16], SiC_f [17,18], MWCNTs [19,20], graphene [21,22], and Al_4SiC_4 [23].

Although the MWCNTs has shown its positive effects on enhancing the SiBCN ceramics [19], the oxidation of the MWCNTs should be improved since the starting oxidation temperature of MWCNTs is as

* Corresponding authors.
E-mail: N. Liao, 2008beijing.ln@163.com;
D. Jia, dcjia@hit.edu.cn

low as 587 ℃ [24]. Therefore, how to prolong the existence of MWCNTs is important. Actually, the formation of SiC coating on the surface of MWCNTs can protect the MWCNTs from oxidation at high temperature. Taguchi *et al*. [25] prepared C–SiC coaxial nanotubes at 1300 ℃ with CNTs and Si as raw materials. Zhou and Seraphin [26] and Morisada *et al*. [27] prepared SiC coated MWCNTs taken SiO as silicon source, and the modified MWCNTs could survive the oxidation test at 650 ℃ in air. In addition, polycarbosilane [24] was also adopted to form SiC_xO_y coating on MWCNTs, which improved the oxidation resistance significantly. In addition to the oxidation resistance, the interface bonding between coated MWCNTs and ceramics matrix should be also focused. Morisada *et al*. [28,29] reported that the SiC coated MWCNTs could increase the hardness of the cemented carbides and the fracture toughness of SiC ceramics. Similarly, Song *et al*. [30] suggested that the SiC coated MWCNTs improved the strength and fracture toughness of reaction bonded silicon carbide obviously. The above works demonstrated that the rough surface of coated MWCNTs would increase adhesion strength, while the specific structures were not observed *in-situ*.

Inspired by these works, the present work was devoted to enhancing Si_2BC_3N ceramics with SiC coated MWCNTs as novel reinforcements. Firstly, the polysilazane was pyrolyzed to form SiC coating on MWCNTs surface. Afterwards, the SiC coated MWCNTs incorporated amorphous Si_2BC_3N powders were sintered by SPS. It was revealed that the SiC coating on MWCNTs can improve the oxidation resistance on the one hand; on the other hand, it provided stronger interconnections between MWCNTs and SiC particles, which eventually improved the mechanical properties and thermal shock resistance of the designed Si_2BC_3N ceramics.

2 Experimental

2. 1 Preparation of SiC coated MWCNTs

In present work, the choice of the precursor must be a liquid with good fluidity and therefore polysilazane was selected [31]. Multi-walled carbon nanotubes (MWCNTs, 95 wt% fixed carbon, Chengdu Organic Chemicals Co., Ltd., China, with outer diameters around 10–30 nm) were impregnated in polysilazane solution (with a DURAZANE 1800 concentration at 0.05 mol/L and taking acetone as solvent) and stirred for 15 min accompanied with sonication. Then the slurries were filtrated and dried at 80 ℃ for 12 h to obtain the precursor coated MWCNTs. Fourier-transform infrared spectra (FTIR) of the specimens were acquired with an IR spectrometer (Bruker Vertex 70). Afterwards, the precursor coated MWCNTs was put into a tube furnace and heated to 1400 ℃ with a holding time of 2 h. The heating rate adopted was 5 ℃/min and Ar (100 mL/min) was adopted to maintain the inert atmosphere.

2. 2 Preparation of Si_2BC_3N–MWCNTs nano composites

The starting raw materials were well crystalline cubic silicon powder (95% in purity, 45.0 μm, Beijing Mountain Technical Development Center, China), hexagonal boron nitride power (98.0% in purity, 0.6 μm, Advanced Technology & Materials Co., Ltd., Beijing, China), and graphite flake (99.5% in purity, 8.7 μm, Qingdao Huatai Lubricant Sealing S&T Co., Ltd., China). According to our previous works, the molar ratio of Si:BN:C was set as 2:1:3 and the ball to powder mass ratio was 20:1 [19]. Then the mixed powders were loaded into the silicon nitride vials along with identical component balls under argon atmosphere and milled by a planetary ball mill (P4, Fritsch GmbH, Germany). The rotation speed of the main disk was set as 350 rpm, and the vials were 600 rpm in reverse. The machine was paused for 10 min every 40 min, and the effective milling time was 20 h.

In the present work, 1 vol% and 2 vol% SiC coated MWCNTs were milled with the amorphous Si_2BC_3N powder. For a uniform distribution of MWCNTs in Si_2BC_3N powder, planetary mill with zirconia vessel and balls were adopted. The ball to powder mass ratio was set as 20:1 here and taken ethanol as milling medium. The MWCNTs and Si_2BC_3N powders were ball milled for 6 h at a speed of 250 rpm to avoid the ZrO_2 contamination. After that, the slurries were dried at 80 ℃ for 24 h for evaporating the ethanol. Correspondingly, the powders were labeled as SCNT1 and SCNT2 respectively. In comparison, the pristine Si_2BC_3N powder was labeled as SCNT0.

2. 3 Spark plasma sintering and characterization

The prepared Si_2BC_3N–MWCNTs powders were loaded into cylindrical graphite die of 40 mm in diameter. A sheet of graphite paper was placed

between the punch and the powder for removing the sample easily out of the die after cooling. The SPS (FCT-HP25) sintering process was conducted under protection of high purity Ar and a uniaxial pressure of 40 MPa was applied throughout the sintering. The sintering temperatures were set at 1900 ℃ at a rate of 100 ℃/min accompanied with a holding time of 5 min. The sintering temperature profiles and variations of shrinkage were kept recording during the sintering process.

The sintered samples were ground and polished with 0.4 μm SiC abrasive paper. The density of samples was measured by the Archimedes method with deionized water as medium. The property measurements were carried out on omnipotence mechanics tester (Instron 5569, Instron Corp., USA) and hardness tester (HVS-5, Laizhou Huayin Testing Instrument Co., Ltd., China). The flexural strength and the Young's moduli were obtained using three-point bending test on 3 mm × 4 mm×20 mm bars with a span of 16 mm and a crosshead speed of 0.5 mm/min. The Young's moduli were calculated through dividing the stresses by the strains obtained from the three-point bending tests. The fracture toughness was determined using the single edge notched beam method with a crosshead speed of 0.05 mm/min, and the testing bar dimension was 2 mm×4 mm×20 mm (16 mm outer span). The depth of the notches was around 2.0 mm and the width was about 0.2 mm (Instron5569, Instron Corp., USA). Four bars were tested for an average value. The Vickers hardness was measured on polished sample surface with a load of 10 kg and a holding time of 15 s. The phases and fracture surface of ceramics were analyzed using X-ray diffraction spectrum (XRD, 40 kV/100 mA, D/max-γB Cu Kα, Rigaku Corp., Japan) and a scanning electron microscopy (SEM, 30 kV, Quanta 200 FEG, FEI Co., USA), respectively. STEM (Talos F200x, 200 kV, FEI Company, USA) was also used to analyze the microstructure details of various Si_2BC_3N ceramics.

The thermal shock behavior of prepared Si_2BC_3N composites was explored using a conventional water-quenching technique [13]. In the present work, ice water bath (0–5 ℃) was adopted for the test. Namely, 20 mm × 4 mm × 3 mm test bars were quickly placed into furnace at air atmosphere and maintained for 10 min at the target temperature to eliminate the temperature gradient. Then the test bars were quickly dropped into the ice water bath paralleled to their length direction to minimize the artificial thermal gradient. The thermal shock resistance was assessed by measuring the residual flexural strength at room temperature using the Instron 5569 testing machine with a crosshead speed of 0.5 mm/min. The water quenching temperature differences (ΔT) was chosen as 1000 ℃ in present work in order to compare with former study. To calculate the thermal shock parameters, the thermal expansion coefficient was evaluated through NETZSCH DIL 402C. The thermal shock related parameters R, R'''', and R_{st} were calculated according to the following formulas [13].

$$R = \frac{\sigma_f \cdot (1-\mu)}{E \cdot \alpha} \tag{1}$$

$$R'''' = \frac{E \cdot \gamma_{WOF}}{\sigma_f^{\,2} \cdot (1-\mu)} \tag{2}$$

$$R_{st} = \sqrt{\frac{\gamma_{WOF}}{\alpha^2 E}} \tag{3}$$

where σ_f is the bending strength, E is Young's modulus, α means thermal expansion coefficient, μ is Poisson's ratio, γ_{WOF} represents the work of fracture over a large area, rather than to initiate fracture.

Besides, oxidation resistance of prepared ceramics was also evaluated and the target oxidation temperatures were set as 1200, 1400, and 1600 ℃ with a holding time of 3 h. After oxidation test, the oxidation layer morphologies and thicknesses were characterized and measured with the help of aforementioned SEM.

3 Results and discussion

3.1 Structural evolutions of SiC coated MWCNTs

Firstly, the FTIR was adopted to characterize the polysilazane coating on MWCNTs and the results were shown in Fig. 1. In comparison with the pristine MWCNTs, the characteristic bands for the Si–H, Si–N, Si–C, C–H, Si–CH_3, and N_2CSi–H groups were acquired for the polysilazane coated MWCNTs. In addition, Si–O–Si groups arose from the reaction of the polysilazane with the moisture during drying process. All these assignments were referenced from literature [32–34]. The FTIR spectra demonstrated the presence of polysilazane coating on MWCNTs.

The microstructures of the MWCNTs with and without SiC coating were observed with SEM and TEM. Figures 2(a) and 2(b) showed that the coating

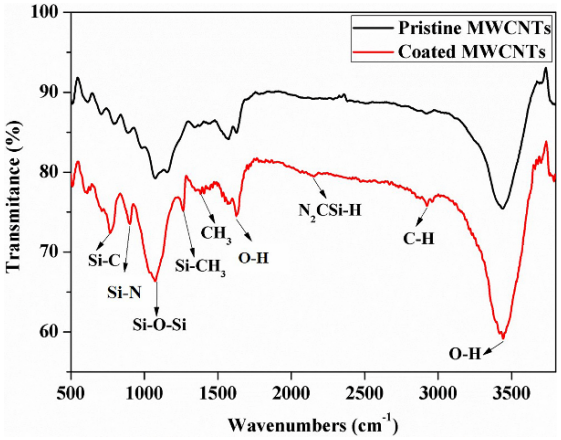

Fig. 1 FTIR spectra of MWCNTs with and without polysilazane coating.

process had no obvious effect on the macroscopic morphology of MWCNTs under SEM observation. In comparison, the TEM micrographs identified the presence of a nano-scaled SiC coating on the surface of MWCNTs (Figs. 2(c) and 2(d)). Furthermore, XRD was adopted to character the phase compositions of the treated MWCNTs. Figure 3(a) suggested that mainly SiC phase was formed in comparison with the pristine MWCNTs. Therefore, it was reasonable to conclude that SiC coating was successfully synthesized on MWCNTs judging from the phase and microstructure characterizations. Generally, mainly SiC and relatively less Si_3N_4 could be formed during the decomposition of polysilazane. However, very less SiC phase and

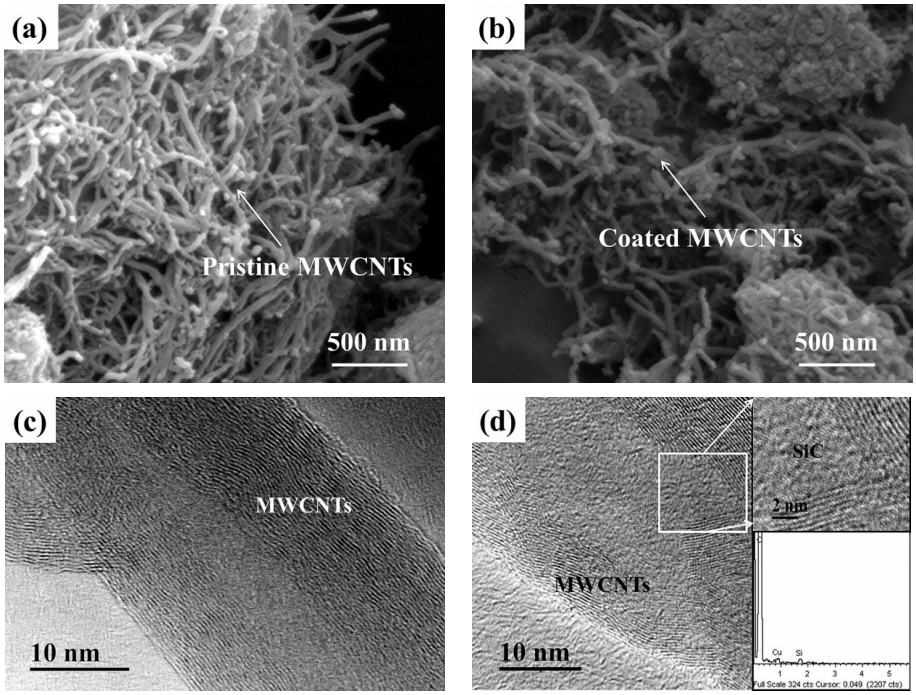

Fig. 2 SEM and TEM pictures of MWCNTS without (a, c) and with (b, d) SiC coating.

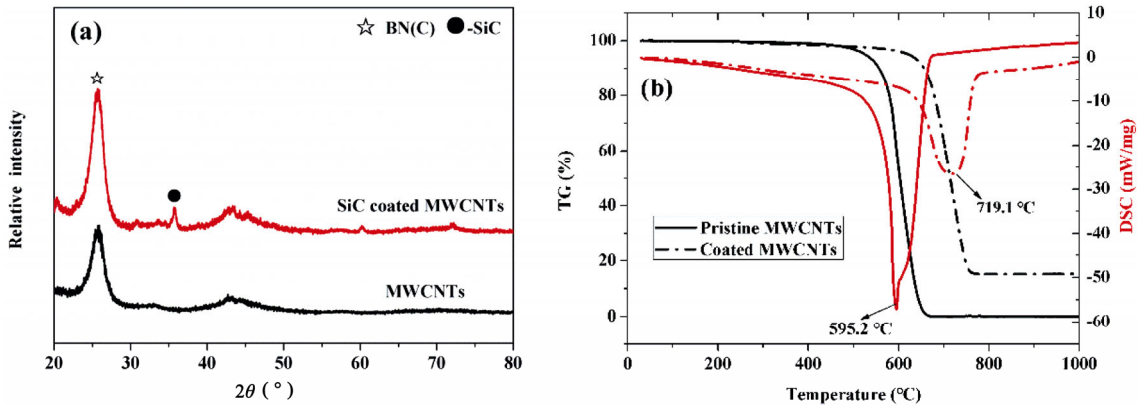

Fig. 3 (a) XRD patterns and (b) TG–DSC curves of MWCNTs with and without SiC coating.

rarely no Si_3N_4 phase were detected in Fig. 3(a). This was because of the presence of only ~20 wt% polysilazane coating on the surface of MWCNTs and the reaction between polysilazane and MWCNTs under high temperature. Besides, Fig. 3(b) showed TG–DSC curves of the MWCNTs with and without coating. The results revealed that the SiC coating was ~15.5 wt% on MWCNTs and it improved the oxidation resistance of MWCNTs obviously (the peak oxidation temperature increased from 595.2 to 719.1 ℃).

3. 2 Phase compositions of Si_2BC_3N ceramics

Figure 4 depicted the XRD patterns of the sintered Si_2BC_3N ceramics. In addition, the XRD pattern showing the amorphous state of pristine Si_2BC_3N was also inserted in Fig. 4. It was obvious to see that the BN(C), 6H–SiC, and 3C–SiC phases were detected in all the specimens. The relative peak intensity of 3C–SiC increased while 6H–SiC decreased gradually with the incorporation of SiC coated MWCNTs. This variation matched well with former result, where the MWCNTs stimulated the formation of 3C–SiC phase [19].

3. 3 Microstructures of Si_2BC_3N ceramics

The fracture surfaces of the prepared Si_2BC_3N ceramics were observed through SEM. The detailed microstructures of specimen SCNT0 were not shown here since they have been described elsewhere [19]. Figures 5(a) and 5(b) showed the microstructures of specimens SCNT1 and SCNT2, respectively. Apparently, the SiC coated MWCNTs were mainly embedded in the matrix. The observation of broken MWCNTs revealed the potential enhancing mechanisms of MWCNTs in the matrix. Comparing with the pristine Si_2BC_3N ceramics [19], the BN(C) and SiC particles were further developed. This microstructure variation

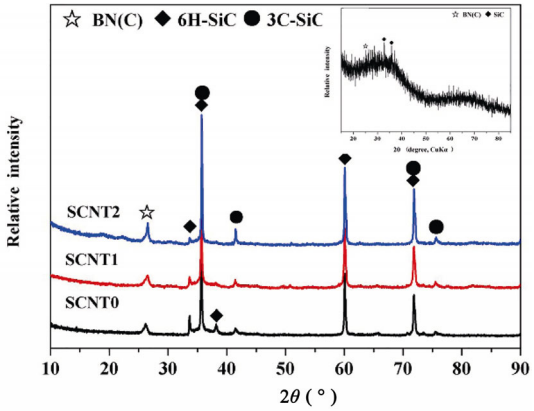

Fig. 4 XRD patterns of Si_2BC_3N ceramics with different content of SiC coated MWCNTs.

is different from the former observation, where the pristine MWCNTs hindered the development of Si_2BC_3N matrix. This should be ascribed to that the SiC coating on MWCNTs acted as crystal nucleus for the development of SiC particles. In addition to the microstructure observation, the cracks propagation paths after an indentation test were presented in Fig. 6. A relatively straight crack propagation path was found in specimen SCNT0 (Fig. 6(a)) and the enlarged image also showed the clear crack propagation. In contrast, much curved crack propagation paths were observed in specimens SCNT1 and SCNT2. The main mechanisms for the formation of curved crack propagation should be attributed to the MWCNTs "pull out" and "crack bridging". According to the former study, these effects would influence the mechanical properties eventually [19].

To better observe the detailed structures of Si_2BC_3N ceramics, TEM was adopted. Figure 7 presented the TEM micrographs of specimen SCNT0. As shown in Fig. 7(a), the SiC particle size was mainly around 100–

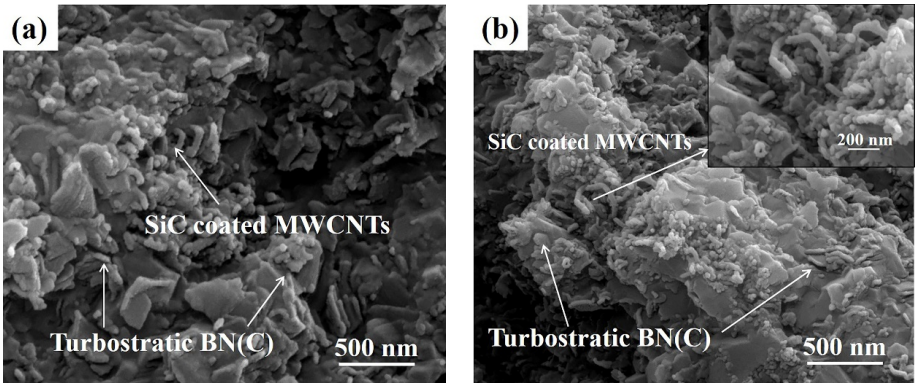

Fig. 5 Micrographs of Si_2BC_3N ceramics: (a) SCNT1; (b) SCNT2.

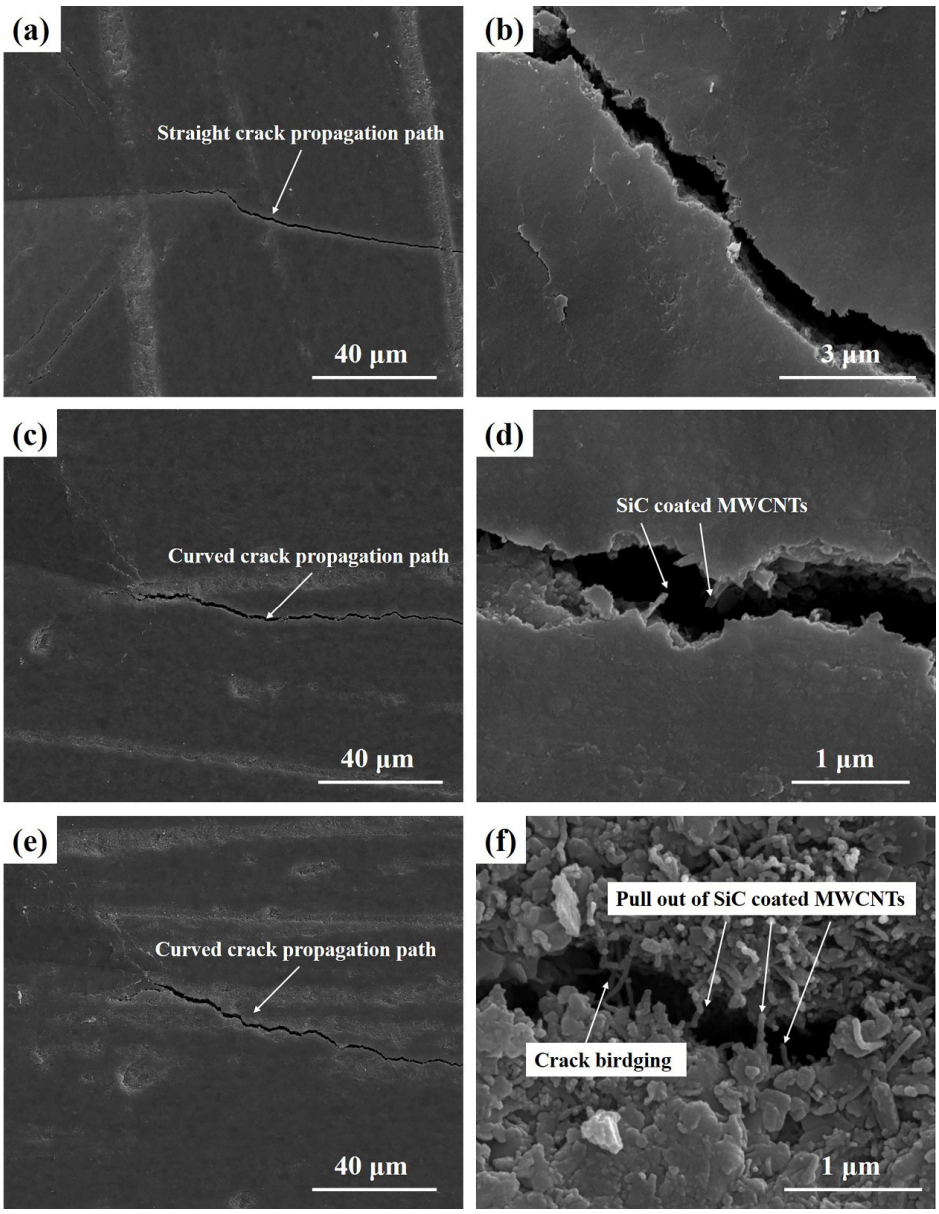

Fig. 6 Crack propagation paths after an indentation test: (a, b) SCNT0; (c, d) SCNT1; (e, f) SCNT2.

200 nm. Meanwhile, Fig. 7(b) showed a representative BN(C) structure, which corresponded to the high-resolution graph of the marked red square shown in Fig. 7(a). Besides, an element mapping was depicted in Fig. 7(c), demonstrating the homogeneous distribution of SiC particles and BN(C) plates [13].

Similarly, Fig. 8 showed the TEM micrographs of specimen SCNT2. Figure 8(a) presented a representative picture of the designed Si_2BC_3N ceramics. Three red squares were marked and the specific structures were further observed. Figure 8(b) revealed the high-resolution graph of SiC particle (square A) with an interplanar spacing of 0.26 nm. Additionally, Fig. 8(c) depicted that one side of the MWCNTs was embedded in the SiC particle (square B). Interestingly, the other side of the MWCNTs cluster (square C) was jointed with other SiC particles (shown in Fig. 8(d)). Meanwhile, it was difficult to define the exact interfaces between SiC particles and MWCNTs, which should be attributed to the presence of nano SiC coating on MWCNTs. In addition, Fig. 8(e) revealed that the SiC particles and BN(C) plates were slightly larger than those observed in pristine Si_2BC_3N ceramics. Based on these SEM and TEM observations, it was reasonable to deduce that the interconnection between MWCNTs and SiC would enhance the Si_2BC_3N ceramics.

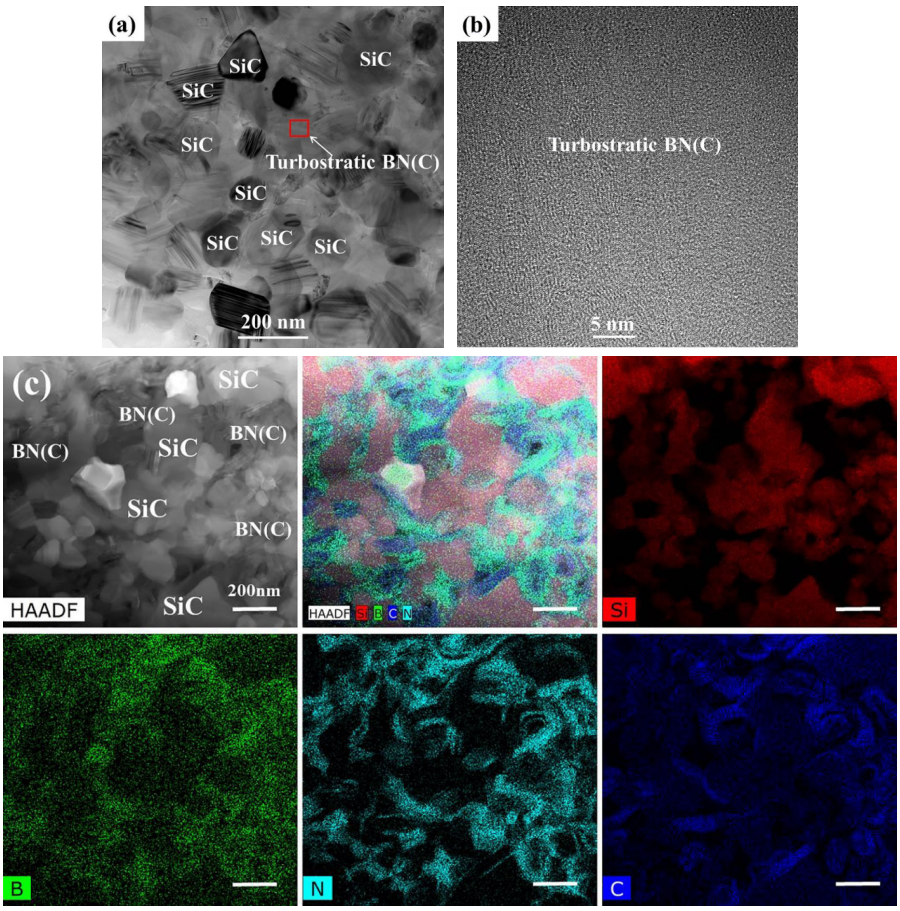

Fig. 7 TEM microstructures of specimen SCNT0; (c) is reproduced with permission from Ref. [13], © Elsevier Ltd and Techna Group S.r.l. 2018.

3. 4 Mechanical properties

Table 1 listed the physical and mechanical properties of prepared Si_2BC_3N ceramics. For better comparison, the properties of 1 vol% pristine MWCNTs enhanced Si_2BC_3N ceramics were also listed together. Firstly, it was obvious that the incorporation of 1 vol% MWCNTs or 1 vol% SiC coated MWCNTs had no apparent effect on the densification behavior. In comparison, the introduction of 2 vol% SiC coated MWCNTs improved the relative density. In addition, the Young's moduli of the pristine MWCNTs and SiC coated MWCNTs incorporated Si_2BC_3N ceramics were higher than the original Si_2BC_3N ceramics. The higher Young's moduli may be induced by the improved relative density. Besides, the flexural strengths of the MWCNTs incorporated composites were much higher than that of the original composites. Among the obtained results, specimen SCNT2 obtained the highest strength at 532.1 MPa due to the enhanced connections between MWCNTs and SiC particles. Additionally, specimen CNT1 also showed a relatively high strength at 462.1 MPa. Comparing with specimen CNT1, specimen SCNT1 showed lower strength, attributing to the fact that the coating process may cause little aggregation of MWCNTs. Furthermore, Table 1 also listed the fracture toughness of the Si_2BC_3N ceramics. Similarly, the MWCNTs with or without SiC coating improved the toughness significantly. With introducing 1 vol% MWCNTs, the toughness increased from 4.11 to 5.54 MPa·m$^{1/2}$. In comparison, 1 vol% SiC coated MWCNTs further improved the toughness to 5.80 MPa·m$^{1/2}$ although specimen CNT1 had higher strength. Furthermore, specimen SCNT2 obtained the highest fracture toughness at 6.66 MPa·m$^{1/2}$. The further enhancement obtained in the SiC coated MWCNTs containing specimens should be ascribed to the interconnections between MWCNTs and SiC particles.

3. 5 Thermal shock resistance calculation and evaluation

In fact, one of the advantages of the introduction of MWCNTs is the improvement on the thermal shock resistance [20]. Therefore, the present work firstly

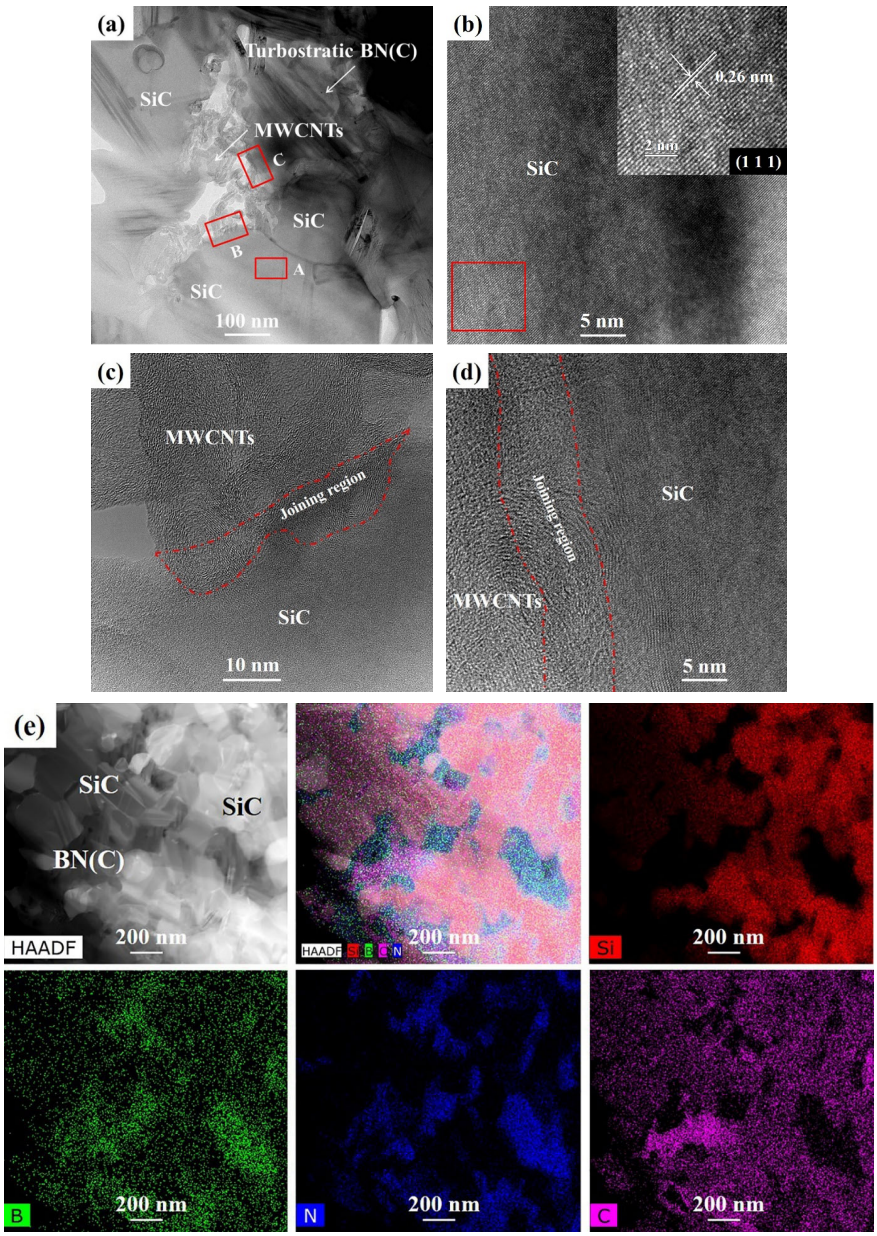

Fig. 8 TEM micrographs of specimen SCNT2. (b, c, d) represent the squares A, B, and C marked in Fig. 8(a), respectively.

Table 1 Physical and mechanical properties of Si_2BC_3N ceramics

Index	Bulk density (g/cm^3)	Relative density (%)	Young's modulus (GPa)	Flexural strength (MPa)	Fracture toughness (MPa·m$^{1/2}$)
SCNT0 [19]	2.58	91.1	106.4±0.6	320.1±25.8	4.11±0.02
CNT1 [19]	2.58	91.2	111.6±0.6	462.1±35.2	5.54±0.45
SCNT1	2.59	91.7	142.5±6.5	390.9±28.6	5.80±0.26
SCNT2	2.61	93.1	144.0±1.8	532.1±22.1	6.66±0.25

calculated the thermal shock related parameters according to classical theory and then evaluated the residual strengths after thermal shock. Table 2 depicted the parameters and tested residual strengths of prepared Si_2BC_3N ceramics. Generally, R parameter was taken to evaluate its thermal shock fracture resistance, and R'''' or R_{st} parameters were applied to indicate the thermal shock damage resistance. The R parameter suggested that both the MWCNTs and SiC coated MWCNTs could improve the cracks initiation resistance,

which was correlated with the flexural strength. Similarly, the thermal stress damage resistance was enhanced with the introduction of MWCNTs with or without SiC coating. R'''' represented the toughness of specimens and it varied in accordance with the fracture toughness. Besides, the thermal shock parameter, R_{st} also suggested that the MWCNTs modified specimens should have better thermal shock resistance.

To verify the theory prediction, the thermal shock test at 1000 ℃ was conducted. In the previous work, the MWCNTs addition improved the residual strength from 93.4 to 101.8 MPa [20]. In comparison, present work showed that the SiC coated MWCNTs could further improve the thermal shock resistance. The residual strengths of specimen SCNT1 and SCNT2 reached 128.3 and 193.0 MPa, respectively. The residual strength of 193.0 MPa at ΔT=1000 ℃ was few reported for Si_2BC_3N ceramics. Comparing with former works, it is certain that the introduction of 2 vol% SiC coated MWCNTs outperformed the 1 mol% Zr–Al [13], the 2 vol% graphene [21], and 5 wt% Al_4SiC_4 [23] additives. The residual strength was significantly improved attributing to the enhanced adhesion strength between SiC coated MWCNTs and Si_2BC_3N matrix.

3. 6 Oxidation resistance

Furthermore, whether the SiC coated MWCNTs can survive the oxidation environment or not was addressed in present work. Figure 9 showed the surface

Table 2 Calculated thermal shock parameters and tested residual strengths of Si_2BC_3N ceramics

Index	R (℃)	R'''' (mm)	R_{st} ($K \cdot m^{1/2}$)	$CMOR_{TS}$ (MPa)	Residual strength ratio (%)
SCNT0 [20]	451	0.18	7.9	93.4±4.3	29.2
CNT1 [20]	615	0.19	10.1	101.8±1.0	22.0
SCNT1	432	0.21	7.3	128.3±16.4	32.8
SCNT2	579	0.24	10.4	193.0±30.6	36.2

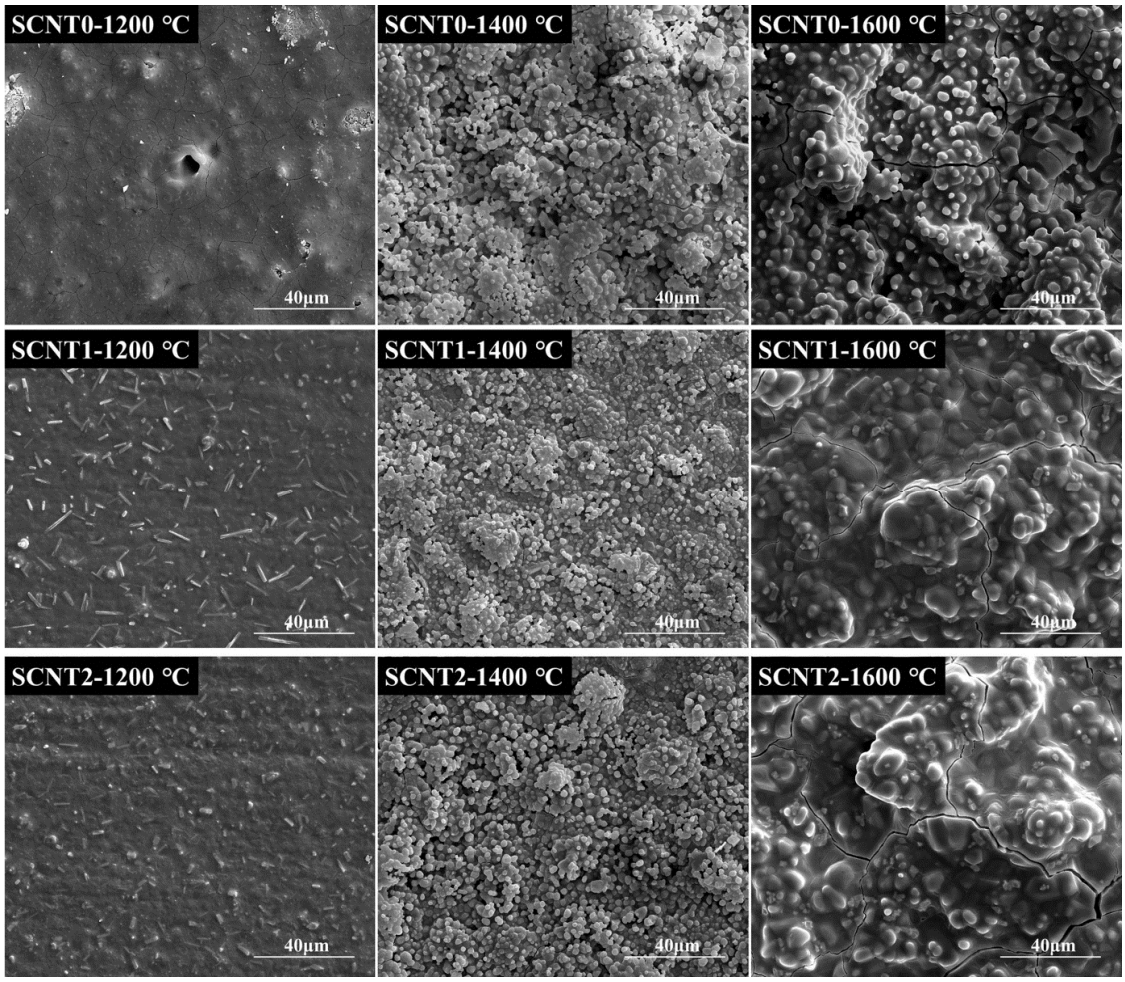

Fig. 9 SEM microstructures of Si_2BC_3N ceramics after oxidation test.

morphologies of the designed Si_2BC_3N ceramics after oxidation tests. At 1200 ℃, dense surfaces were observed for all the specimens. In comparison, some stacked SiO_2 particles were observed in the specimens tested at 1400 ℃. The formation of pores should be ascribed to the evaporation of B_2O_3 and SiO gas during the oxidation process. Similarly, specimens SCNT1 and SCNT2 presented denser surface structures after oxidation test at 1600 ℃. In general, the SiC coated MWCNTs containing specimens showed relative denser structure. Besides the surface morphologies, the cross-sections of oxidation layers were measured and depicted in Fig. 10. Based on the obtained results, the designed Si_2BC_3N ceramics exhibited relatively higher oxidation resistance than the pristine Si_2BC_3N ceramics. The increased relative density and improved oxidation resistance of SiC coated MWCNTs contributed to the improved oxidation resistance of designed Si_2BC_3N ceramics. Generally, the addition of SiC coated MWCNTs has no negative effects on the oxidation resistance of Si_2BC_3N ceramics. In fact, the oxidation resistance of SCNT2 is relatively lower than that of SCNT1 under high temperature, considering of the oxidation layer thickness and cross-section microstructure.

3. 7 Discussion

The above results demonstrated that the prepared SiC coated MWCNTs had better enhancing effects than the pristine MWCNTs. The detailed mechanisms will be further discussed in the following part. Firstly, the existence of MWCNTs under high temperature is critical important since no enhancement can be achieved if MWCNTs was burned out during the application. Therefore, nano-scaled SiC coating was successfully synthesized through pyrolyzing polysilazane in present work. Based on the thermal analysis, the oxidation resistance of the coated MWCNTs has been obviously improved. Afterwards, the SiC coated MWCNTs modified Si_2BC_3N ceramics were sintered with SPS. Generally, the mechanical properties have close

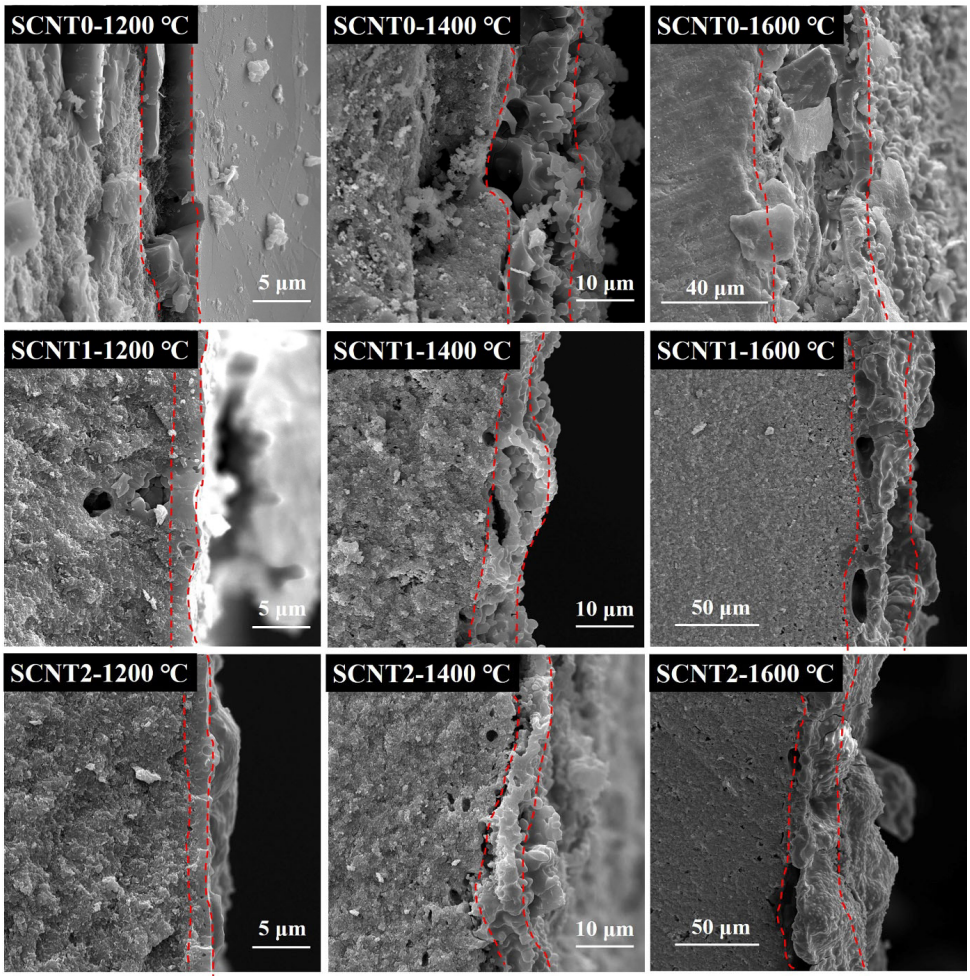

Fig. 10 Oxidation layer thickness of Si_2BC_3N ceramics after oxidation test.

relationship with the relative density and microstructure development. In the present work, the introduction of SiC coated MWCNTs improved the relative density slightly. But above all, the enhanced mechanical properties should be attributed to the developed microstructures. The general enhancing mechanisms of MWCNTs should be "crack bridging", "crack deflection", and "pull out" as described elsewhere [19]. Nevertheless, the present work achieved even better properties than those of the pristine MWCNTs enhanced Si_2BC_3N ceramics. According to the TEM observation, part of the interconnections should be chemical bonding, which should be stronger than the physical adhesion. Therefore, it was reasonable to conclude that interconnections between SiC coated MWCNTs and SiC particles contributed to the higher flexural strength and fracture toughness. Besides, the cracks initiation and propagation were also suppressed due to the increased adhesion strength among the ceramics composites. Consequently, the breaking of MWCNTs and the interfaces debonding between MWCNTs and SiC would consume larger energy, leading to higher stress resistance. Meanwhile, the "pull out" of rough MWCNTs cluster between SiC particles would also contribute to more energy dissipation mechanisms.

4 Conclusions

Based on the above investigations, the following conclusions can be drawn:

(1) SiC coated MWCNTs could be synthesized with taking polysilazane as precursor. The formed nano-scaled SiC coating improves the peak oxidation temperature of MWCNTs from 595.2 to 719.1 ℃.

(2) An interconnection structure between SiC coated MWCNTs and SiC particles can further enhance the ceramics composites significantly. Therefore, the flexural strength and fracture toughness of the SiC coated MWCNTs enhanced Si_2BC_3N ceramics test at ambient temperature, are much higher than those of the pristine Si_2BC_3N ceramics and the 1 vol% MWCNTs enhanced Si_2BC_3N ceramics, attributing to the enhanced interface adhesion strengths.

(3) The SiC coated MWCNTs modified Si_2BC_3N ceramics have higher cracks initiation and propagation resistance due to the optimized interface bonding. Therefore, the residual strength of the 2 vol% SiC coated MWCNTs reinforced Si_2BC_3N ceramics is 193.0 MPa after thermal shock test at 1000 ℃. Furthermore, the SiC coated MWCNTs modified Si_2BC_3N ceramics possess relatively better oxidation resistance than the pristine Si_2BC_3N ceramics when being tested at 1200 and 1400 ℃ in air.

Acknowledgements

This work was supported financially by National Natural Science Foundation of China (NSFC, Grant Nos. 51702065 and 51621091) and China Postdoctoral Science Foundation (Grant No. 2018M631924).

References

[1] Riedel R, Kienzle A, Dressler W, *et al*. A silicoboron carbonitride ceramic stable to 2000 ℃. *Nature* 1996, **382**: 796–798.

[2] Tavakoli AH, Gerstel P, Golczewski JA, *et al*. Effect of boron on the crystallization of amorphous Si–(B–)C–N polymer-derived ceramics. *J Non-Cryst Solids* 2009, **355**: 2381–2389.

[3] Schiavon MA, Sorarù GD, Yoshida IVP. Poly(borosilazanes) as precursors of Si–B–C–N glasses: synthesis and high temperature properties. *J Non-Cryst Solids* 2004, **348**: 156–161.

[4] Jia DC, Liang B, Yang ZH, *et al*. Metastable Si–B–C–N ceramics and their matrix composites developed by inorganic route based on mechanical alloying: fabrication, microstructures, properties and their relevant basic scientific issues. *Prog Mater Sci* 2018, **98**: 1–67.

[5] Yang ZH, Jia DC, Duan XM, *et al*. Effect of Si/C ratio and their content on the microstructure and properties of Si–B–C–N Ceramics prepared by spark plasma sintering techniques. *Mat Sci Eng A* 2011, **528**: 1944–1948.

[6] Zhang PF, Jia DC, Yang ZH, *et al*. Progress of a novel non-oxide Si–B–C–N ceramic and its matrix composites. *J Adv Ceram* 2012, **1**: 157–178.

[7] Wang JY, Duan XM, Yang ZH, *et al*. Ablation mechanism and properties of SiC_f/SiBCN ceramic composites under an oxyacetylene torch environment. *Corros Sci* 2014, **82**: 101–107.

[8] Miao Y, Yang ZH, Zhu QS, *et al*. Thermal ablation behavior of SiBCN–Zr composites prepared by reactive spark plasma sintering. *Ceram Int* 2017, **43**: 7978–7983.

[9] Miao Y, Yang ZH, Rao JC, *et al*. Influence of sol-gel derived ZrB_2 additions on microstructure and mechanical properties of SiBCN composites. *Ceram Int* 2017, **43**: 4372–4378.

[10] Zhang PF, Yang B, Lu Z, *et al*. Effect of AlN and ZrO_2 on the microstructure and property of the 2Si–B–3C–N ceramic. *Ceram Int* 2018, **44**: 3406–3411.

[11] Li DX, Yang ZH, Jia DC, *et al*. Preparation, microstructures, mechanical properties and oxidation resistance of SiBCN/ZrB_2–ZrN ceramics by reactive hot pressing. *J Eur Ceram Soc* 2015, **35**: 4399–4410.

[12] Ye D, Jia DC, Yang ZH, *et al*. Microstructures and mechanical properties of SiBCNAl ceramics produced by mechanical alloying and subsequent hot pressing. *J Zhejiang Univ Sci A* 2010, **11**: 761–765.

[13] Liao N, Jia DC, Yang ZH, *et al*. Enhanced mechanical properties, thermal shock resistance and oxidation resistance of Si_2BC_3N ceramics with Zr–Al addition. *Mat Sci Eng A* 2018, **725**: 364–374.

[14] Liang B, Yang ZH, Jia DC, *et al*. Densification, microstructural evolution and mechanical properties of Si–B–C–N monoliths with LaB_6 addition. *J Alloys Compd* 2017, **696**: 1090–1095.

[15] Liang B, Yang ZH, Miao Y, *et al*. Microstructural evolution, mechanical and thermal properties of LaB_6 embedded in Si–B–C–N prepared by spark plasma sintering. *Ceram Int* 2017, **43**: 4814–4820.

[16] Liang B, Yang ZH, Li YT, Yuan, *et al*. Ablation behavior and mechanism of SiC_f/C_f/SiBCN ceramic composites with improved thermal shock resistance under oxyacetylene combustion flow. *Ceram Int* 2015, **41**: 8868–8877.

[17] Li DX, Wu DX, Yang ZH, *et al*. Effects of in situ amorphous graphite coating on ablation resistance of SiC fiber reinforced SiBCN ceramics in an oxyacetylene flame. *Corros Sci* 2016, **113**: 31–45.

[18] Wang JY, Yang ZH, Duan XM, *et al.* Microstructure and mechanical properties of SiC_f/SiBCN ceramic matrix composites. *J Adv Ceram* 2015, **4**: 31–38.

[19] Liao N, Jia DC, Yang ZH, *et al*. Strengthening and toughening effects of MWCNTs on Si_2BC_3N ceramics sintered by SPS technique. *Mat Sci Eng A* 2017, **710**: 142–150.

[20] Liao N, Jia DC, Yang ZH, *et al*. Enhanced thermal shock and oxidation resistance of Si_2BC_3N ceramics through MWCNTs incorporation. *J Adv Ceram* 2018, **7**: 276–288.

[21] Li DX, Yang ZH, Jia DC, *et al*. Microstructure, oxidation and thermal shock resistance of graphene reinforced SiBCN ceramics. *Ceram Int* 2016, **42**: 4429–4444.

[22] Li DX, Yang ZH, Jia DC, *et al*. Spark plasma sintering and toughening of graphene platelets reinforced SiBCN nanocomposites. *Ceram Int* 2015, **41**: 10755–10765.

[23] Liao N, Jia DC, Yang ZH, *et al.* Mechanical properties and thermal shock resistance of Si_2BC_3N ceramics with ternary Al_4SiC_4 additive. *Ceram Int* 2018, **44**: 9009–9017.

[24] Luo M, Li YW, Jin SL, *et al*. Oxidation resistance of multi-walled carbon nanotubes coated with polycarbosilane-derived SiC_xO_y ceramic. *Ceram Int* 2011, **37**: 3055–3062.

[25] Taguchi T, Igawa N, Yamamoto H, *et al*. Preparation and characterization of single-phase SiC nanotubes and C–SiC coaxial nanotubes. *Physica E* 2005, **28**: 431–438.

[26] Zhou D, Seraphin S. Production of silicon carbide whiskers from carbon nanoclusters. *Chem Phys Lett* 1994, **222**: 233–238.

[27] Morisada Y, Maeda M, Shibayanagi T, *et al*. Oxidation resistance of multi-walled carbon nanotubes coated with silicon carbide. *J Am Ceram Soc* 2004, **87**: 804–808.

[28] Morisada Y, Miyamoto Y. SiC-coated carbon nanotubes and their application as reinforcements for cemented carbides. *Mat Sci Eng A* 2004, **381**: 57–61.

[29] Morisada Y, Miyamoto Y, Takaura Y, *et al*. Mechanical properties of SiC composites incorporating SiC-coated multi-walled carbon nanotubes. *Int J Refract Met H* 2007, **25**: 322–327.

[30] Song N, Liu H, Fang JZ. Fabrication and mechanical properties of multi-walled carbon nanotube reinforced reaction bonded silicon carbide composites. *Ceram Int* 2016, **42**: 351–356.

[31] Liu J, Qiao YL, Zhang P, *et al*. Synthesis of SiC ceramics from polysilazane by laser pyrolysis. *Surf Coat Technol* 2017, **321**: 491–495.

[32] Günthner M, Wang K, Bordia RK, *et al*. Conversion behaviour and resulting mechanical properties of polysilazane-based coatings. *J Eur Ceram Soc* 2012, **32**: 1883–1892.

[33] Nguyen VL, Zera E, Perolo A, *et al*. Synthesis and characterization of polymer-derived SiCN aerogel. *J Eur Ceram Soc* 2015, **35**: 3295–3302.

[34] Zera E, Nickel W, Kaskel S, *et al*. Out-of-furnace oxidation of SiCN polymer-derived ceramic aerogel pyrolized at intermediate temperature (600–800 ℃). *J Eur Ceram Soc* 2016, **36**: 423–428.